Sustainable Cities and Society 44 (2019) 666–675

Contents lists available at ScienceDirect

Sustainable Cities and Society

journal homepage: www.elsevier.com/locate/scs

Quantifying the seasonal contribution of coupling urban land use types on Urban Heat Island using Land Contribution Index: A case study in Wuhan, China

Qiuping Huang[a], Jiejun Huang[a,*], Xining Yang[b], Chuanglin Fang[c], Youjia Liang[a]

[a] Department of Regional Planning and Management, School of Resource and Environmental Engineering, Wuhan University of Technology, Wuhan 430070, China
[b] Department of Geography and Geology and Institute for Geospatial Research and Education, Eastern Michigan University, Ypsilanti, MI 48197, USA
[c] Institute of Geographic Sciences and Natural Resources Research, CAS, Beijing 100101, China

ARTICLE INFO

Keywords:
Urban Heat Island (UHI)
Land Contribution Index (LCI)
Land use types
Land surface temperature
Urbanization
Remote sensing

ABSTRACT

Urban Heat Island (UHI) is an urban climate phenomenon which is expected to respond to the change of urban environment and land use types in the future. UHI is closely related to urbanization and urban land use changes, since the expansion of impervious surface greatly affects the thermodynamic properties of the underlying surface. New ways to measure and assess the inner quantitative relationship between land use types and UHI are thus critical to answer the questions in this field. This paper presents a new method for better quantifying the contribution of respective land use type on UHI with the proposed Land Contribution Index (LCI). Seasonal thermal contribution of each land use type to UHI can be calculated based on the difference in average temperatures between a certain land use type and the entire study area. The experiment was conducted in Wuhan, China during 2005–2015 when the city was in rapid urbanization. Results indicate that the UHI effect has become more prominent in areas of rapid urbanization in the study area, and strong UHI (including high level and extremely high level) accounted for 8.56% of the whole region in 2015 compared with 2005 (3.35%). In addition, through analyzing temporal and spatial patterns of the distribution of UHI, increasing UHI areas were mainly distributed in the central and western parts of the city during 2005–2009, and then migrated to the surroundings from 2011. Furthermore, based on the calculation of LCI, construction land had the highest contribution to the UHI effect in the summer of 2015, while water body had conversely the lowest contribution to the UHI effect in the spring of 2005. Urban green space including forest land and agricultural land had intensively negative contributions to the UHI effect, and their alleviating functions on the thermal environment were less remarkable in winter.

1. Introduction

Since the mid-20th century, urbanization has become one of the most significant human activities (Pickett et al., 2011). Extensive urban population influx and consequent shifts from green space to impervious surface often lead to urban/rural ecological imbalances (Aguilar, 2008; Li, Liu, Huisingh, Wang, & Wang, 2016), with study demonstrating that generalized urbanization alters the process of energy and water balance, and affects the dynamics of air flow (Oke, 1995). Therefore, in order to ensure the safety and comfort of rapidly growing urban population, it is necessary to reinforce our understanding about the urban climate and the processes affecting it (Gaur, Eichenbaum, & Simonovic, 2018).

The difference between urban and rural temperatures, commonly known as the Urban Heat Island (UHI), is one typical urban climate phenomenon that has been investigated in the past (Rizwan, Dennis, & Liu, 2008). This phenomenon usually happens with the development of urbanization, when changes in the thermal properties of urban underlying surface result in high temperatures in central urban areas and low temperatures in suburbs. The characteristic of the UHI effect has been extensively studied in the past two decades. A typical study by Mihalakakou, Flocas, Santamouris, and Helmis, (2002) investigated the effect of the synoptic-scale atmospheric circulation on the UHI over Athens for two years, and found that the high pressure ridge mostly favors the heat island phenomenon. In 2003, progress in urban climatology over the two decades was reviewed, and meantime the diversity

* Corresponding author.
E-mail addresses: huang_qiuping@whut.edu.cn (Q. Huang), hjj@whut.edu.cn (J. Huang), xyang5@emich.edu (X. Yang), fangcl@igsnrr.ac.cn (C. Fang), yjliang@whut.edu.cn (Y. Liang).

https://doi.org/10.1016/j.scs.2018.10.016
Received 10 May 2018; Received in revised form 14 September 2018; Accepted 9 October 2018
Available online 29 October 2018
2210-6707/ © 2018 Elsevier Ltd. All rights reserved.

of UHI depending of the medium sensed and the sensing technique was explained (Arnfield, 2003). Furthermore, UHI was later researched by scholars from different regions. The relationship between landscape characteristics and UHI in Phoenix, Arizona was assessed using landscape metrics (Connors, Galletti, & Chow, 2013), and the characteristics of UHI in Nicosia, Cyprus was also estimated using multiyear urban and rural climatic data and analysis (Theophilou & Serghides, 2015).

Although many efforts have been achieved, studies on the UHI are still limited to a few areas (Jin, Dickinson, & Zhang, 2005) due to the size and density of the population, the level of industrialization, the seasonal climate and the traffic patterns of different cities (Busato, Lazzarin, & Noro, 2014; Charabi & Bakhit, 2011; Xiong et al., 2012). In addition, traditional UHI research relied mainly on meteorological stations and numerical models because of data acquisition deficiencies. Gallo, Easterling, and Peterson, (1996) analyzed the meteorological data and investigated that the difference of daily temperature in urban areas was lower than that in rural space. Wilby (2003) predicted the UHI effect in London using numerical UHI models and revealed that London's UHI was most intense near the centre of the city, during nighttime, in summer, and under stable weather.

In recent years, consistent and extensive spatial coverage has made satellite-based remote sensing datasets accessible in the study of urban physics and climatology, which provides a direct and convenient way to determine the UHI effect combined with Geographical Information System (GIS) technique (Odindi, Bangamwabo, & Mutanga, 2015). Remote sensing datasets are ideal for applying consistent definitions and methodologies to the UHI studies of cities across the globe, such as NOAA's Advanced Very High Resolution Radiometer (AVHRR) data, Landsat's Thematic Mapper (TM) and Enhanced Thematic Mapper (ETM) data, Medium Resolution Imaging Spectrometer (MERIS) data, and Advanced Spaceborne Thermal Emission and Reflection Radiometer (ASTER) data (Arino et al., 2007; Cai, Du, & Xue, 2011; Holderness, Barr, Dawson, & Hall, 2013; Joshi et al., 2015). Among these, MODIS dataset is preferred by researchers due to its high temporal resolution (twice daily) and large data abundance at moderate spatial resolution (Odindi et al., 2015). For example, two types of UHI were analyzed to monitor the spatial and temporal evolution of surface and air heating using MODIS data (Anniballe, Bonafoni, & Pichierri, 2014). Surface urban heat island (SUHI) intensities for two tropical urban areas in Brazil were also explored using remote sensing data obtained from MODIS sensor (Flores, Pereira Filho, & Karam, 2016).

Furthermore, the relation between the UHI intensity and land use types has been extensively researched in recent years. The change of land use types is the most direct manifestation of rapid urbanization, leading to the alteration of physical characteristics of the earth's surface and affecting the exchange of energy between the surface and the atmosphere (Yuan & Bauer, 2007). Different land use characteristics have significant impacts on the thermal environment in urban areas. The shift from rural to urban land use types can affect temperature trends similar to that in a greenhouse warming scenario (Fall et al., 2010). Moreover, previous studies have also indicated that urban land use types and their related thermal impacts have incredibly heterogeneous features. Xian and Crane (2006) quantitatively determined urban land use extents and development densities to investigate urban surface thermal patterns in Tampa Bay and the Las Vegas valley. Moreover, the relation between land surface temperature and land use category was analyzed in Shanghai, China. The result indicated that not only land cover patterns, but also other anthropogenic forces can affect urban UHI (Li et al., 2014).

Despite many efforts have been achieved in the UHI research, the coupling relationship between the UHI effect and land use types remains uncertain thus requires more quantitative analyses. In addition, UHI has been hypothesized as a leading factor of urban natural disaster which leads to heavy rains in flood seasons as well as the regional flood in metropolitan cities in China such as Wuhan City. This provides an excellent opportunity as a study area to investigate the coupling effect on UHI because the land use types in Wuhan has undergone great changes in the first decade of the 21st century. In this paper, we will study the changes of land use characteristics in Wuhan city in a decade period, and explore the coupling impact of such changes on the UHI intensities and spatial patterns in the study area. Furthermore, we proposed a new indicator called Land Contribution Index (LCI) in order to better quantify the contribution of different land use types to the UHI effect.

The specific objectives of this work are: (1) to derive land use structures from the Landsat TM/ETM + remote sensing images and obtain land surface temperature from the MODIS dataset for the period 2005–2015 in Wuhan; (2) to divide the UHI intensity into different levels according to the universal UHI intensity grading criterion; (3) to analyze the temporal and spatial patterns of the UHI along with their changes over the study period; and (4) to explore the relationship between land use types and the UHI, and to quantify the contribution of respective land use type to the UHI effect using the proposed LCI indicator.

2. Materials and methods

2.1. Study area and data

Wuhan is the capital city of Hubei Province, China (29°58′—31°22′N, 113°41′—115°05′E). It is situated in the eastern part of Jianghan Plain and the middle reaches of the Yangtze River. Wuhan is a metropolitan city in the central China area, and is also a significant transport interchange. The city covers an area of 8494 km^2, with 13 municipal districts and 3 state-level development zones, accounting for 4.6% of the total area of Hubei Province. At the end of 2016, the resident population in Wuhan reached 10.76 million. It has a subtropical humid climate with an average annual temperature of 15.8℃ ~ 17.5℃, and the climate type of Wuhan belongs to "subtropical humid climate" according to Koppen classification. As a traditional industrial city, urbanization in Wuhan ranks forefront in China, with the consequent urban heat island effect and significant air pollution (Xie & Zhou, 2015). Urban land use extent has also remarkably increased in the first decade of the 21st century in this city, resulting in high temperatures in central urban areas and low temperatures in suburbs. Fig. 1 shows the relative location and the enlarged image of Wuhan city respectively.

To quantitatively measure land surface temperature and compare the UHI intensity in the study area, MODIS datasets (MODLT1F: 1 km surface temperature monthly synthetic datasets in China) from 2005 to 2015 were acquired with the temporal resolution of three month. Taking year 2005 as example, we prepared the MODIS data from Jan. 1, 2005; Apr. 1, 2005; Jul. 1, 2005 and Oct. 1, 2005 for our analysis to represent four seasonal land surface temperatures in 2005. We also collected the Landsat-5 TM images for 2005 (Jul.25) and the Landsat-8 OLI TIRS images for 2015 (Jul.29) with a spatial resolution of 30 m, which have been registered to the Universal Transverse Mercator (UTM) coordinate system. In addition, an administrative division vector map of Wuhan at a scale of 1:1,000,000 was used along with the remote sensing images to obtain detailed land use classification information.

2.2. Data pre-processing

The processing platforms of remote sensing data, administrative vector data, and MODIS temperature data are mainly ArcGIS and ENVI software in this study. The first processing step was the projection transformation, where the images and the administrative map were projected under a unified projection; the second step was to complete the preprocessing of the images, including cropping, splicing and merging. Through the method of supervised classification (Melgani & Bruzzone, 2004), we categorized land use types of Wuhan city into five categories according to the urban land use classification system (Table 1). Then the land use data of two years were converted into

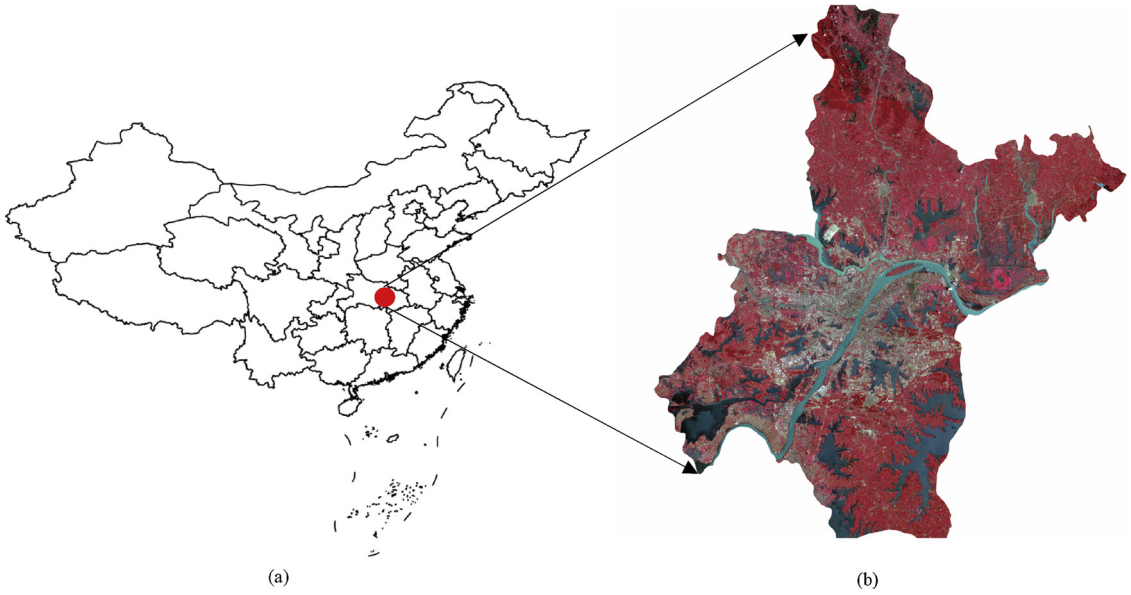

Fig. 1. Location of Wuhan city in China: (a) relative location of Wuhan; and (b) the enlarged remote sensing image of the city.

vector format and overlaid with the administrative layer in order to obtain the city's urban land use maps in 2005 and 2015 respectively.

In order to derive land surface temperature in the study area, we processed the time-series MODIS data in ArcGIS by cropping and merging. Specifically, land surface temperature of four seasons (January corresponds to winter, April to spring, July to summer and October to autumn) in 2005, 2007, 2009, 2011, 2013 and 2015 were obtained respectively for subsequent calculation of the UHI intensity.

2.3. Derivation of the urban heat island intensity

In this study, land surface temperature of Wuhan was obtained directly from the MODLT1F datasets in different years. The MODIS sensor is a critical instrument aboard NASA's Terra and Aqua satellites (Wang et al., 2012). The MODIS-Terra determines the earth surface's temperature based on split window algorithm from thermal and mid-infrared bands at a resolution of 1 km (Guillevic et al., 2012). To minimize the influence of cloud noise, we chose almost cloud-free (maximum cloud volume only reaches 0.36%) 1 km monthly land surface temperature (LST) MODLT1F imagery available. Furthermore, the LST of the study area was extracted from the imagery by clipping.

From the perspective of UHI, the mean LST in rural areas was applied to represent the mean LST in the whole study region in order to obtain the difference in temperature between urban and rural areas. Combined with land use maps, the average LST for each land use types can be computed, and the UHI intensity can be indicated by the difference in LST between urban and surrounding areas (Zhang et al., 2013). The UHI intensity can be calculated as:

$$UHIER = \Delta T / T_s = (T_i - T_s)/T_s \quad (1)$$

Where: *UHIER* refers to the UHI intensity index, expressed in relative LST in the area; ΔT represents the difference between the LST of the *i*-th pixel (T_i) and the mean LST of rural areas (T_s). Subsequently, based on the overall understanding of the spatial and temporal pattern of UHI, the UHI intensity can be categorized into five levels (Table 2).

Table 1
The urban land use classification system.

First Level Classes	Second Level Classes	Descriptions
Agricultural land	–	Cultivated lands for crops, including mature cultivated land, newly-cultivated land, reclamation land, shifting cultivated land; crop land in which a crop is a dominant species and land that is used for intercropping such as crop-fruiter; other lands that have been shifted to cultivation temporarily.
	Paddy field	Arable land that has enough water supply and irrigation facilities for the cultivation of paddy rice and other aquatic crops.
	Dry land	Arable land with no water supply and irrigation facilities; arable land that is used for planting dry farming crops with natural precipitation.
Forest land	–	Lands growing trees, including arbor, shrub, bamboo, and for forestry use.
	Forest	Natural or planted forests with tree canopy cover > 30%.
	Shrub	Lands covered by trees under 2 m high with canopy cover ≥40%.
	Others	Lands, including sparse woodland and nurseries; lands with the growth of herbs-based land.
Construction land	–	Lands used for settlements, business use, factories, transportation infrastructures, and so on.
	Residential land	Lands used for urban and rural settlements and their ancillary facilities.
	Business land	Lands used for business use, including wholesale and retail land, accommodation land, financial land, and so on.
	Others	Lands used for industrial and mining use, public administration, and public service and lands used for transportation facilities such as airports.
Water body	–	Lands covered by natural water bodies or lands with facilities for water reservation.
	Reservoir	Man-made facilities with a total storage capacity more than 10 million cubic meters.
	Lakes and rivers	Lands covered by lakes or rivers, including canals.
Unused land	–	Lands are not utilized or hard to make use of.
	Sandy land	Lands with a surface of sand cover, with no more than 5% vegetation cover.
	Bare land	Bare land with exposed soil or rocks, basically with no vegetation cover.
	Saline land	Lands with saline accumulation and sparse vegetation.
	Undeveloped land	New lands in towns or villages that have not been put into use yet.

Table 2
The UHI intensity levels.

Value of *UHIER* (℃)	Level	Description
$UHIER \leq 0$	Extremely low	Extreme low temperature zone, meaning the LST difference between urban and rural areas is marginal.
$0 < UHIER \leq 0.1$	Low	Low temperature zone, meaning the LST difference between urban and rural areas is slight.
$0.1 < UHIER \leq 0.2$	Medium	Medium temperature zone, meaning the LST difference between urban and rural areas is moderate.
$0.2 < UHIER \leq 0.3$	High	High temperature zone, meaning the LST difference between urban and rural areas is great.
$0.3 < UHIER$	Extremely high	Extreme high temperature zone, meaning the LST difference between urban and rural areas is intensively great.

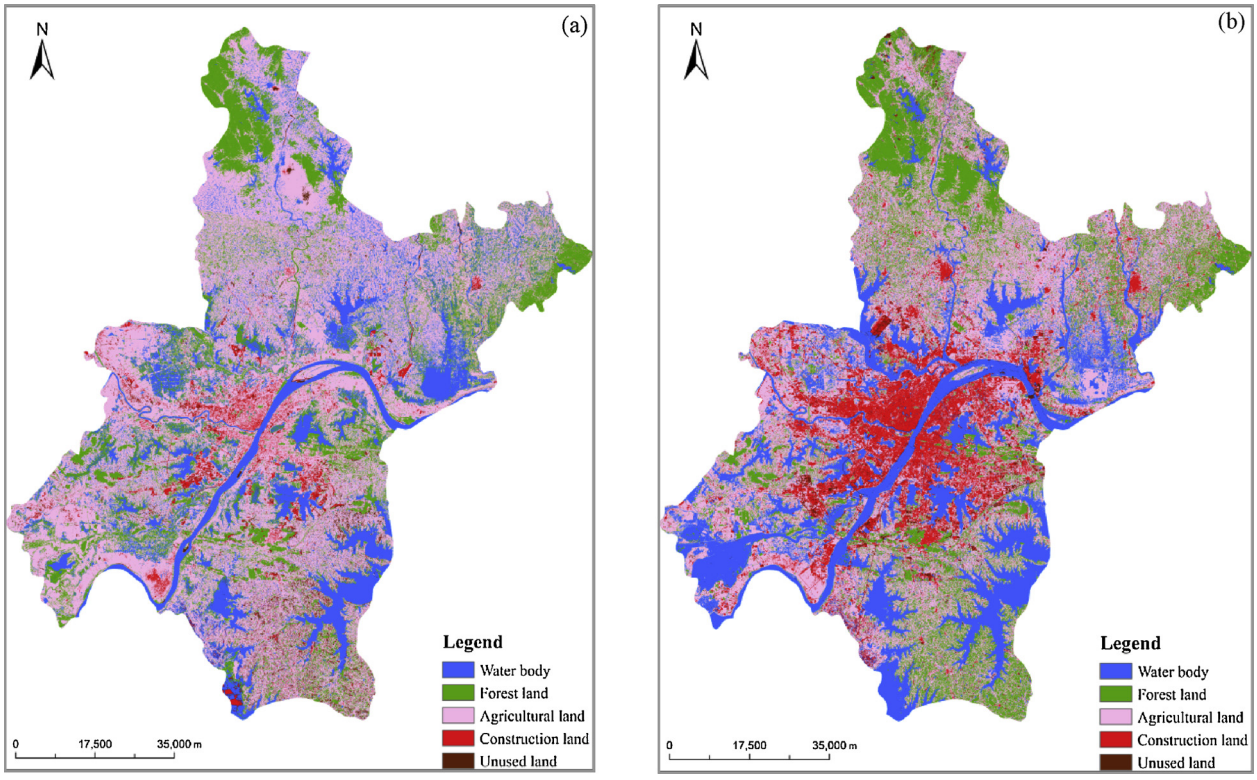

Fig. 2. Urban land use classification map obtained from satellite imagery for Wuhan: (a) land use map in 2005; and (b) land use map in 2015.

2.4. Calculation of the land contribution index (LCI)

In order to better quantify the relationship between urban land use types and their impact on the UHI effect, the contribution of respective land use type is defined in this study. Urban land use types of the study area in 2005 and 2015 were acquired according to Table 1 respectively (Fig. 2), and then post classification smoothing was conducted on land use maps to remove noisy pixels (Chen, Zhao, Li, & Yin, 2006). The classification accuracy was then assessed by comparing the classified land use types with the original map. The sampling points were randomly taken across the study area and relatively uniformly distributed among all land use types as references to test classification accuracy, and the overall accuracy in this experiment is over 90%.

To determine the contribution of different land use types in affecting the UHI, over 2500 (500 for each land use type) distributed points were randomly extracted from each of the land use type. “Generate random point” tool in ArcGIS software was applied in this experiment for extracting the whole sample points, and for ensuring random selection and coverage of the points. In this study, the range of sample points from 200 to 800 (for each land use type) was investigated for deriving the land surface temperature. We figured out that the number of sample points had little impact on the calculation of average temperature, but 500 for each type were enough to satisfy the maximum coverage of the study area without overflowing points. These points were then used to extract their corresponding land surface temperature values for different seasons. In case of possible seasonal temperature changes and atmospheric conditions during the acquisition of temperature (Sastry & Barua, 2017), the temperature means of all land use types in relation to the entire urban landscape for each of the season were calculated separately. Take the mean seasonal temperature for all land use types in the area as the baseline, the seasonal thermal impact of each land use type on the entire area can be defined by the LCI as follows:

$$LCI_i = (T_i - M) \times P_i\ ,\ i = 1,2,3,4,5 \quad (2)$$

Where: T_i is the average temperature of the i-th land use type, M is the average temperature of the entire study area, and i represents five land use types; P_i refers to the proportion of the i-th land use type to the entire area; LCI is a quantitative indicator for determining the thermal contribution of respective land use type to the UHI effect in different seasons. If LCI ≥ 0, the corresponding land use type has a positive effect on promoting the UHI; on the contrary, LCI value below 0 indicates that the corresponding land use type is alleviated to the UHI.

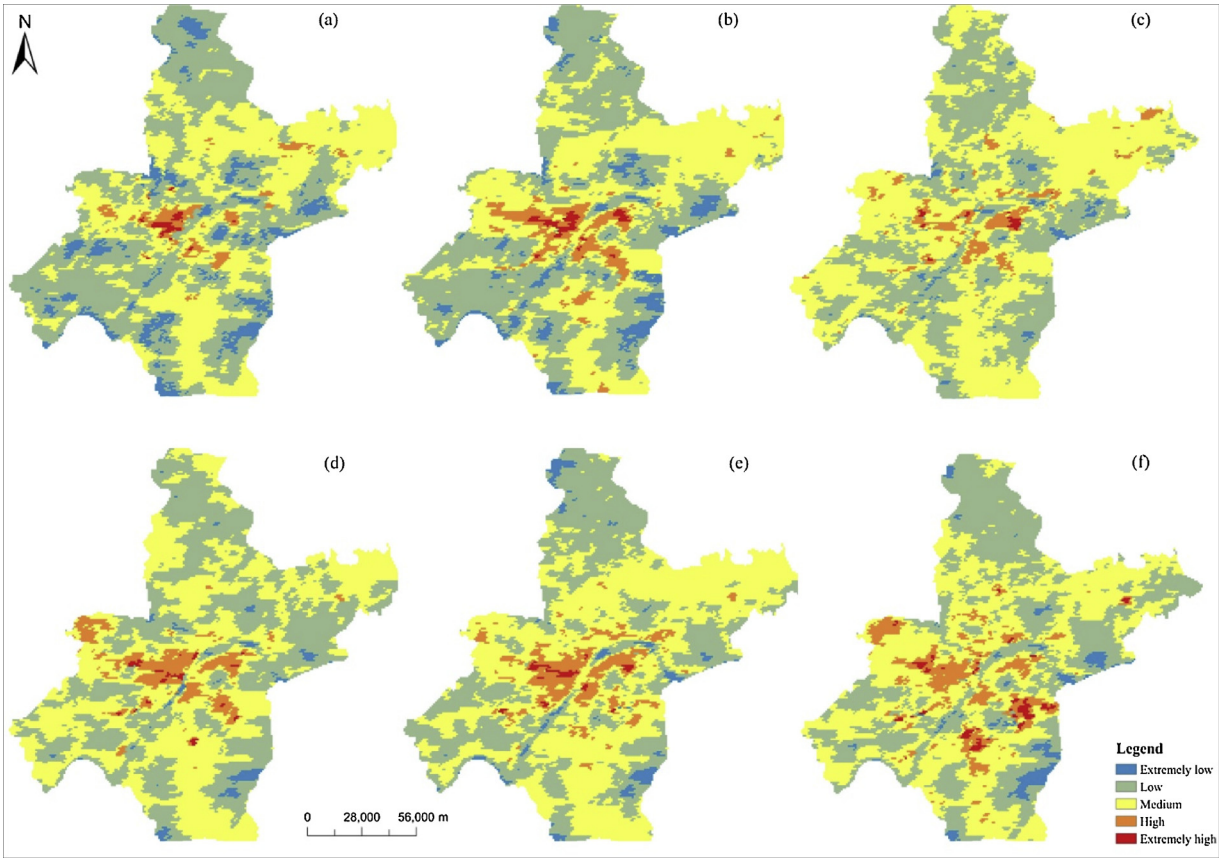

Fig. 3. UHI grading maps in the study area during 2005–2015 at an interval of two years, (a) - (f) refers to the UHI grading map obtained for 2005, 2007, 2009, 2011, 2013 and 2015 respectively.

3. Results and discussion

3.1. Analyzing spatial and temporal characteristics of the UHI effect in Wuhan

3.1.1. Classification of the UHI intensity

We obtained the UHI maps of the study area according to Eq. (1) and categorized the UHI intensity into five levels based on Table 2. In addition, we selected the LST of same period each year (Jul. 1) to derive the UHI maps from 2005 to 2015 at a two-year interval, which avoided seasonal impact on the UHI. Fig. 3 shows the UHI maps with their corresponding levels in respective year, and the proportion of each UHI intensity level was summarized in Table 3.

It is noted from above figures and charts that, the area of UHI in the study area had been expanding in the period of 2005–2015, while a slight drop happened in 2009. The UHI effect nearly covered the whole city with varying levels, except for the northwest corner, which has a high coverage of forest (see Fig. 2). In 2005, the overall UHI effect in the study area is relatively weak, with only 3.35% strong UHI areas. Compared with 2005, the percentage of strong UHI almost doubled in 2007 and decreased moderately to about 4.45% in 2009. According to "Wuhan Statistical Yearbook", the extreme maximum temperature in 2007 was 39.1 ℃, and the figure in 2006 and 2009 was 37.5 ℃ and 37.2 ℃ respectively. Continuous high temperature in the summer of 2007 may explain the steep rise of the percentage of strong UHI (6.42%) in the chart. Since 2009, the UHI effect in the study area kept growing, which might be relevant to the rapid urbanization of Wuhan in the early 21st century. According to a previous report, urbanization impacts impervious surfaces that alter sensible and latent heat fluxes, environmental issues such as UHI effect emerge with urbanization subsequently (Mahmood et al., 2014). Strong UHI accounts for over 8.56% of the whole region in 2015, indicating that the city was experiencing an intensive UHI effect.

From the perspective of spatial changes, UHI areas are mainly distributed on east and west sides of the Yangtze River from the beginning. Then the areas radiated to the surroundings gradually with the intensities getting higher. Compared with land use maps (Fig. 2), we can also see that extreme low temperature and weak UHI effect always

Table 3
Classification of UHI levels and their counted area in Wuhan during 2005–2015.

Year	UHI intensity levels with corresponding area (pixels)					
	Extremely low	Low	Medium	High	Extremely high	Strong UHI percentage (including high level and extremely high level)
2005	1829	10820	9223	659	100	3.35%
2007	1487	10192	9507	1274	179	6.42%
2009	358	9014	12259	941	66	4.45%
2011	377	9799	11032	1314	85	6.19%
2013	573	8607	11810	1512	123	7.23%
2015	673	9310	10637	1716	215	8.56%

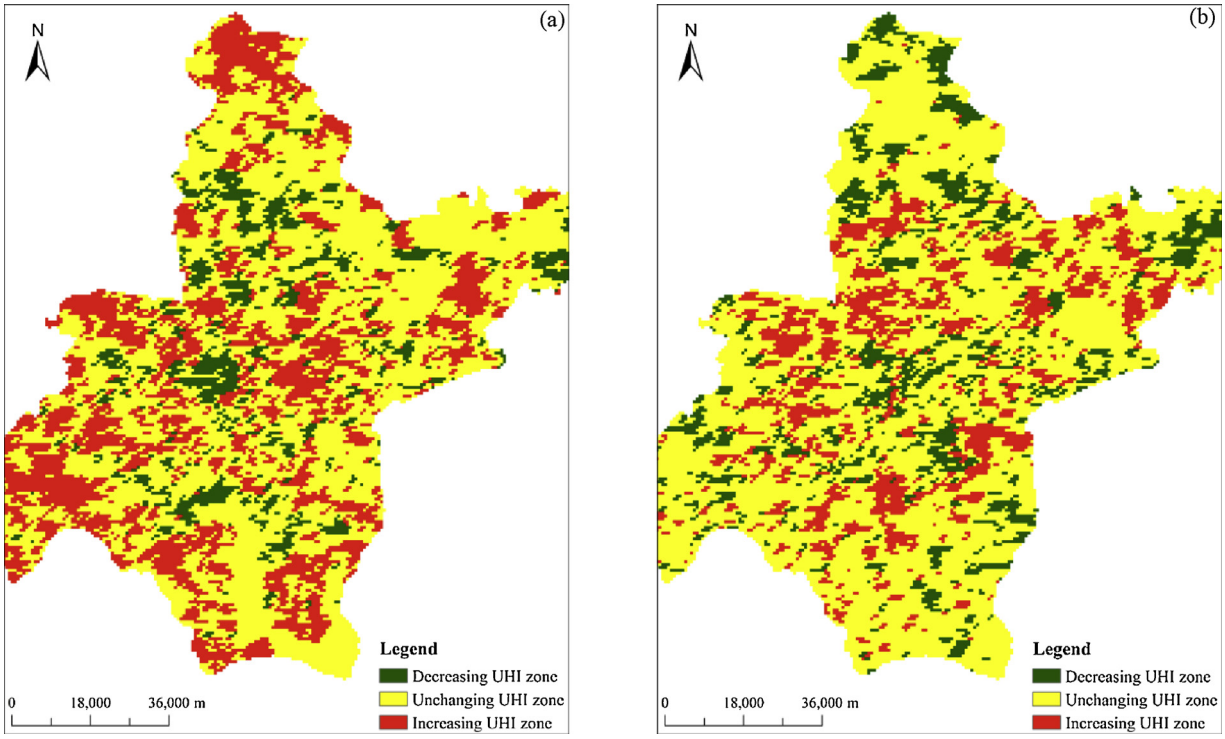

Fig. 4. Spatial-temporal changes of the UHI intensity in Wuhan during the period of 2005–2015: (a) presents the spatial-temporal changing patterns of the UHI from 2005 to 2009; and (b) presents the same scene from 2011 to 2015.

occurred at the water body. The UHI effect on forest land is also weaker than other areas, demonstrating that water body and forest land are alleviated to the UHI. Previous studies point out that UHI is associated with a decline in urban green spaces (Oliveira, Andrade, & Vaz, 2011), and the loss of green space leads to a reduction in heat loss from latent heat flux (Screen and Simmonds, 2010). However, whether water body and forest have a negative effect on the UHI and what levels they can achieve in reducing the UHI effect are waiting to be discussed in the Sec.3.2.

3.1.2. Analysis of temporal and spatial patterns of the UHI

In order to better describe the temporal and spatial changes of the UHI in Wuhan, differential operation was conducted on the UHI grading maps. Two maps were then obtained to reflect spatial-temporal changes of the UHI intensity and the variation between different years. Fig. 4a shows the spatial-temporal changing patterns of the UHI in the period of 2005–2009, Fig. 4b shows that in the period of 2011-2015. We categorized the change of UHI into three types: increasing UHI zone, decreasing UHI zone and unchanging zone. The proportion of each zone is shown in Table 4.

Fig. 4 presents the spatial-temporal changes of UHI in Wuhan, meaning that the UHI intensity experienced a significant growth during 2005-2009. Increasing UHI areas were distributed mainly in the central and western regions of the city (Fig. 4a), which was relevant to the urbanization of Wuhan. Central area is the core of this city covering all kinds of modernization, urbanization in Wuhan also originated in the central area and then spurred the development of surrounding regions. The increasing UHI zone accounted for 31.12% of the whole city in the period of 2005–2009, since land use types in Wuhan has undergone great changes in the first decade of the 21st century. At the beginning of the next decade, only 17% of the study area was witnessing a growing UHI effect. In contrast, the percentage of decreasing UHI areas rose to 14.63% in 2015. It can be inferred that a significant urbanization process occurred in Wuhan in the first decade of the 21st century, which not only contributed to the changes of land use types, but also affected the UHI effect. After 2011 the process of urbanization shifted from the city center to the surroundings in Wuhan, the increasing UHI effect was therefore evenly concentrated on urban surroundings in space.

Table 4
Proportion of UHI changes in the study area.

Period	Increasing UHI zone	Unchanging zone	Decreasing UHI zone
2005-2009	31.12%	58.80%	10.08%
2011-2015	17.00%	68.37%	14.63%

3.2. Quantifying the relationship between land use types and UHI in the study area based on LCI

3.2.1. Calculating the LCI of each land use type

We tabulated the spatial extents and proportions of different land use types in 2005 and 2015 respectively for calculating the LCI (Table 5). Table 5 shows that agricultural land, water body and forest land were dominant landscapes in the study area in this period. However, it is noticeable that the construction land increased from 7.34% to 12.48%, which was consistent with the ongoing urbanization at that time. The other point needs to be specified is about the change of water body. The Landsat TM/ETM images we chose for classifying land use types in this experiment were on 25/07/2005 and 29/07/2015 respectively. The flood season of Wuhan generally occurs in July and August, and the torrential rain on 23/07/2015 called “7.23 Wuhan Rainstorm” led to a substantial rise in water volume in the whole city (according to Wuhan Meteorological Bereau). Therefore, the percentage of water body in 2015 (23.15%) was much higher than the figure in 2005 (18.71%). In addition, the reduction of forest land, agricultural land and unused land as well as the increase of construction land appeared to be the drivers of the UHI effect in this decade.

Over 2500 (500 for each land use type) distributed points were randomly extracted from each of the land use type using “Generate random point” tool in ArcGIS, which ensured random selection and coverage of the sample points. These points were then used to extract

Table 5
Spatial extents and proportions of land use types in the study area (unit: pixel).

Year	Total	Land use types and their corresponding proportions (%)									
		Water body		Construction land		Agricultural land		Forest land		Unused land	
		Area	Percent	Area	Percent	Area	Percent	Area	Percent	Area	Percent
2005	9324728	1744737	18.71%	684860	7.34%	5104882	54.75%	1554622	16.67%	235627	2.53%
2015	9324646	2158963	23.15%	1163676	12.48%	4214827	45.20%	1656253	17.76%	130927	1.41%

Table 6
Deviations between four seasonal temperature means and respective land type means in 2005.

Land use type	Temperature means in four seasons and their deviations with each land type (℃)			
	Spring	Summer	Autumn	Winter
Water body	−1.98	−1.34	−1.49	−0.81
Construction land	1.24	1.07	0.44	0.26
Agricultural land	−0.47	−0.25	−0.46	−0.14
Forest land	−0.75	−0.52	−0.91	−0.26
Unused land	0.47	0.33	0.36	0.16

Table 7
Deviations between four seasonal temperature means and respective land type means in 2015.

Land use type	Temperature means in four seasons and their deviations with each land type (℃)			
	Spring	Summer	Autumn	Winter
Water body	−1.69	−1.13	−0.63	−1.18
Construction land	0.95	1.49	0.92	0.12
Agricultural land	−0.02	−0.17	−0.11	−0.22
Forest land	−0.27	−0.54	−0.50	−0.29
Unused land	0.69	0.94	0.38	0.03

their corresponding land surface temperature values for different seasons. Then the temperature means of all land use types in relation to the entire urban landscape for each of the season were calculated separately in two years (Table 6).

3.2.2. The relationship between urban land use types and the UHI effect in the study area

The contribution of different land use types to the UHI can be calculated according to Table 5–7 and the LCI of each land use type in 2005 and 2015 is presented in Fig. 5.

Fig. 5 demonstrates a fact that construction land and unused land had positive effects on the UHI effect, in which construction land provided the most significant amount of heat to the study area in four seasons. With the promotion of urbanization process in 10 years, 12.48% of the area was constructed in 2015, which exerted a higher contribution to the UHI effect compared with 7.34% in 2005. In contrast, water body, forest land and agricultural land were alleviated to the UHI effect. Among the three types, water body provided maximum suppression to the UHI effect. The maximum LCI of water body was -0.37 and -0.39 in two years, indicating that temperature variation over water tends to be less variable due to its high heat capacity. Similarly, urban green space including forest land and agricultural land had obvious negative impact on the UHI. The LCI of agricultural land in 2005 was much higher than that of forest land, but in 2015 they had little difference in heat contribution due to the changes of agriculture land (9% decreased) to other land types (refer to Table 5). Urban green space has the function of absorbing toxic gases and purifying the environment, moreover, it can improve local microclimate to compensate for the natural environmental features damaged by urbanization (Bilgili & Gökyer, 2012; Huong & Pathirana, 2013).

Different land use types also represented varying degrees of contribution to the UHI with the change of season. For example, construction land had the greatest heat contribution in spring in 2005 at 0.09, while the same occasion occurred in summer in 2015 with the LCI of 0.187. A similar inconsistency was noted in forest land, which provided the most negative impact on the UHI in spring 2005 and in summer 2015 respectively. We can conclude from Fig. 5 that the greatest contribution of respective land use type to the UHI effect occurred basically in spring in 2005; by contrast, in 2015 most of the heat contribution took place in summer except for water body. As expected, construction land had a high LCI in spring, summer and autumn, which was significantly lower in winter due to lower solar radiation (Oleson, Bonan, & Feddema, 2010). Apart from construction land, the other types also provided less heat contribution in winter. These observations can be explained by the rainfall season of spring and summer which leads to more vibrant urban green space and therefore more heat sinking. In drier winter, the dropping vitality of green space results in the weakening of heat sinking ability (Sharifi, Sivam, & Boland, 2016).

As indicated above, urbanization contributed the most to the increasing temperature and aggravating UHI effect in the study area during this period, as well as the potentially high contribution to global warming. On the contrary, water body and urban green space had obviously negative seasonal heat contributions to the UHI effect. Although some measures can be taken to alleviate the UHI effect and its impact on ecological environment, the increase of urban green space is the most practicable. According to Tan and Li (2013), the average LST for green space was 5.32 K lower than that for commercial and residential land, and the green space size affected the cool island intensity in Beijing. In another related study, Zölch, Maderspacher, Wamsler, and Pauleit, (2016) found that tree planting had the strongest impact on the reduction of average physiological equivalent temperature (PET) at 13% compared with existing vegetation.

Furthermore, the spatial center of the UHI at each level was calculated in this experiment and then overlaid on the land use map in respective year (Fig. 6).

Extremely low level of UHI intensity was concentrated on the surface of water body, and its location nearly kept unchanged during this decade. This phenomenon was consistent with the above description which indicated that temperature variation over water tends to be less variable due to its high heat capacity. Similarly, the spatial center of high and extremely high levels of UHI intensity was consistently distributed on the surface of construction land. The location, however, migrated a little from the city center to the west in 2015. This was also in line with the development of urbanization in Wuhan, which spurred to surroundings in later years.

In contrast, centers of low and medium levels experienced great changes in both location and land use surface. Low level of UHI intensity was situated in the south-west corner, and then migrated to the north-west corner. The change conformed to the spatial variation shown in Fig. 6, showing that the amount of forest land had an obvious increase in the south-west corner of the study area in 2015. Since urban greenery has intensive negative contributions to the UHI, it is reasonable for explaining the migration of the location. Another fact can be

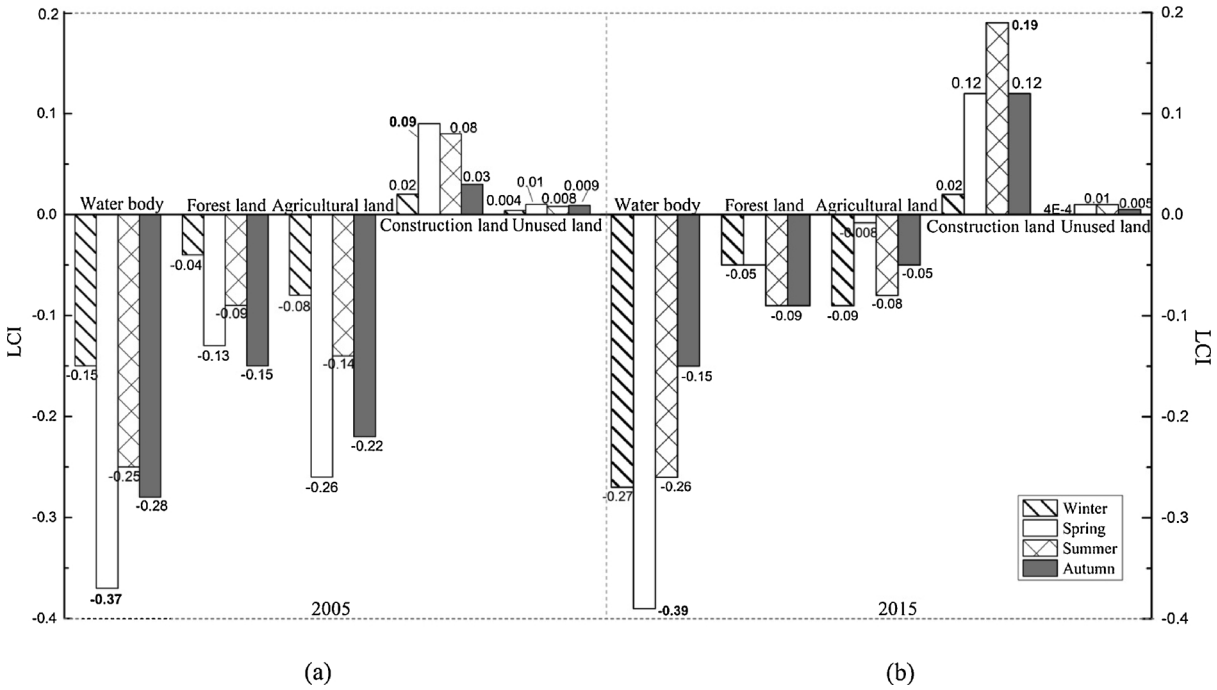

Fig. 5. Land Contribution Index of each land use type in four seasons in the study area. (a), (b) refer to the LCI of five land use types in 2005 and 2015 respectively.

seen on the maps is the change of medium level of UHI intensity. In 2005, the center of medium UHI was fixed on the agricultural surface, and then it migrated to the surface of moderately constructed land after 10 years with the urbanization.

4. Conclusions

In this paper, we proposed an indicator called Land Contribution Index to better quantify the relationship between urban land use types and UHI effect. The experiments were conducted on Wuhan, a metropolitan city with high level of UHI owing to rapid urbanization since the early 21st century. Several conclusions can be made: (1) the area of UHI in the study area had been expanding in the period of 2005–2015, and strong UHI (including high level and extremely high level) accounts for 8.56% of the whole region in 2015, which was more than twice the figure for 2005 (3.35%). (2) Through analyzing temporal and spatial patterns of the distribution of UHI in the study area, increasing UHI areas were mainly distributed in the central and western parts of the

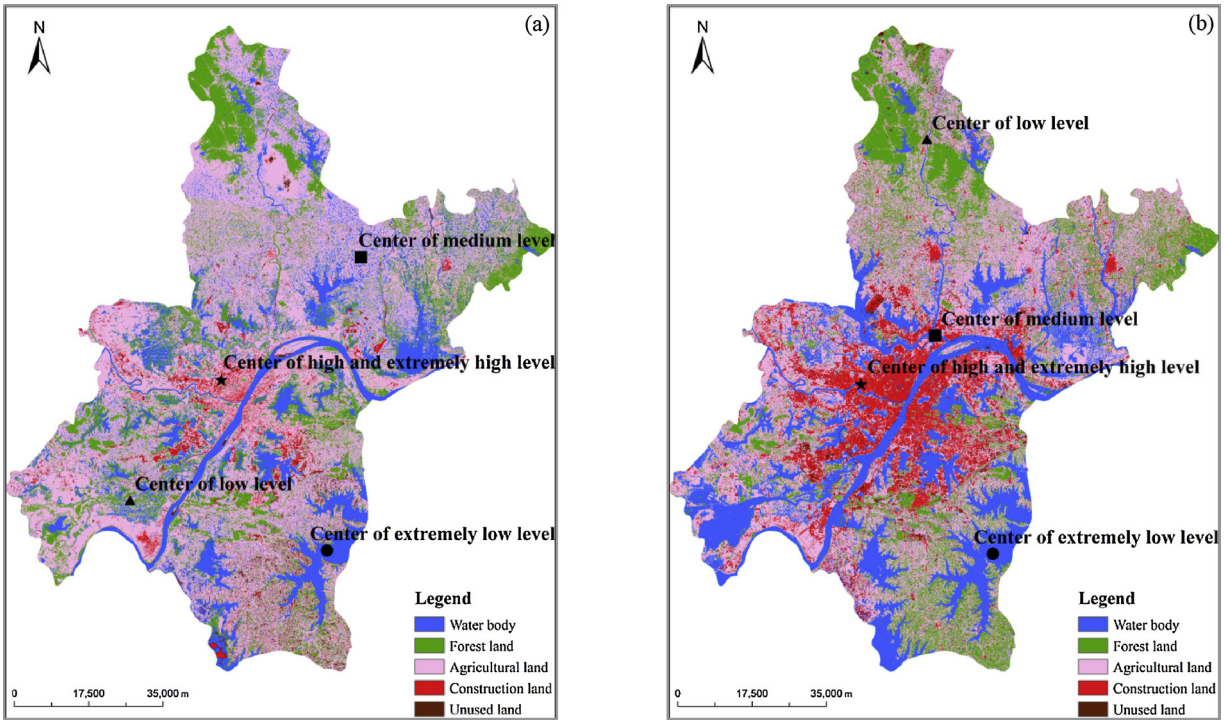

Fig. 6. The spatial center of each UHI intensity level presented in urban land use map: (a) centers of respective UHI intensity level in 2005; and (b) centers of respective UHI intensity level in 2015.

city in the period of 2005–2009, and then migrated to the surroundings during 2011-2015. In addition, the proportion of increasing UHI areas reduced from 31% to 17% in the second half of the study period. (3) Based on the calculation of LCI index of each land use type, construction land had the highest contribution to the UHI effect in the summer of 2015, while water body had conversely the lowest contribution to the UHI effect in the spring of 2005. The growing contribution of construction land was consistent with the corresponding expanding constructed surface, but temperature variation over water tends to be less variable due to its high heat capacity. (4) Urban green space including forest land and agricultural land had intensively negative contributions to the UHI effect, and their alleviating functions on the thermal environment were less remarkable in winter. Extensive urbanization leads to urban ecological imbalances, and the UHI effect derived from urbanization is also related to climatic damages such as heavy rains in developed cities. Based on the guidance of our experimental results, scientific instructions are available for the rational planning and allocation of land resources for policymakers.

We have to acknowledge the limitation of our study given the fact that all the analyses in this paper were based on the interpretation of remote sensing images, by which we investigated not only the UHI phenomenon but also the quantitative relationship between UHI and urban land use types in the study area. In the future study, several works need to be further explored. The derivation of land surface temperature of Wuhan in this experiment was from seasonal MODIS MODLT1F datasets, we will consider other alternative satellite imageries in next stage to reduce the influence of thin cloud and inhomogeneous atmosphere condition. Moreover, it should be also important to explore the effect of human activities and other social-economic factors on the contributions of UHI effect.

Declaration of interest

None.

Acknowledgements

This work was supported by the CRSRI Open Research Program (CKWV2018499/KY), and the National Natural Science Foundation of China (No. 41601184, 41071104).

References

Aguilar, A. G. (2008). Peri-urbanization, illegal settlements and environmental impact in Mexico city. *Cities, 25*, 133–145. https://doi.org/10.1016/j.cities.2008.02.003.

Anniballe, R., Bonafoni, S., & Pichierri, M. (2014). Spatial and temporal trends of the surface and air heat island over Milan using MODIS data. *Remote Sensing of Environment, 150*, 163–171. https://doi.org/10.1016/j.rse.2014.05.005.

Arino, O., Gross, D., Ranera, F., Leroy, M., Bicheron, P., Brockman, C., et al. (2007). GlobCover: ESA service for global land cover from MERIS. *Proccedings of the International Geoscience and Remote Sensing Symposium*. https://doi.org/10.1109/IGARSS.2007.4423328.

Arnfield, A. J. (2003). Two decades of urban climate research: A review of turbulence, exchanges of energy and water, and the urban heat island. *International Journal of Climatology: A Journal of the Royal Meteorological Society, 23*, 1–26. https://doi.org/10.1002/joc.859.

Bilgili, B. C., & Gökyer, E. (2012). Urban green space system planning. In M. Ozyavuz (Ed.). *Landscape planning* (pp. 107–123). TechOpen.

Busato, F., Lazzarin, R. M., & Noro, M. (2014). Three years of study of the urban heat island in Padua: Experimental results. *Sustainable Cities and Society, 10*, 251–258. https://doi.org/10.1016/j.scs.2013.05.001.

Cai, G. Y., Du, M. Y., & Xue, Y. (2011). Monitoring of urban heat island effect in Beijing combining ASTER and TM data. *International Journal of Remote Sensing, 32*, 1213–1232. https://doi.org/10.1080/01431160903469079.

Charabi, Y., & Bakhit, A. (2011). Assessment of the canopy urban heat island of a coastal arid tropical city: The case of Muscat, Oman. *Atmospheric Research, 101*, 215–227. https://doi.org/10.1016/j.atmosres.2011.02.010.

Chen, X. L., Zhao, H. M., Li, P. X., & Yin, Z. Y. (2006). Remote sensing image-based analysis of the relationship between urban heat island and land use/cover changes. *Remote Sensing of Environment, 104*, 133–146. https://doi.org/10.1016/j.rse.2005.11.016.

Connors, J. P., Galletti, C. S., & Chow, W. T. (2013). Landscape configuration and urban heat island effects: Assessing the relationship between landscape characteristics and land surface temperature in Phoenix, Arizona. *Landscape Ecology, 28*, 271–283. https://doi.org/10.1007/s10980-012-9833-1.

Fall, S., Niyogi, D., Gluhovsky, A., Pielke, R. A., Kalnay, E., & Rochon, G. (2010). Impacts of land use land cover on temperature trends over the continental United States: Assessment using the North American Regional Reanalysis. *International Journal of Climatology: A Journal of the Royal Meteorological Society, 30*, 1980–1993. https://doi.org/10.1002/joc.1996.

Flores, J. L., Pereira Filho, A. J., & Karam, H. A. (2016). Estimation of long term low resolution surface urban heat island intensities for tropical cities using MODIS remote sensing data. *Urban Climate, 17*, 32–66. https://doi.org/10.1016/j.uclim.2016.04.002.

Gallo, K. P., Easterling, D. R., & Peterson, T. C. (1996). The influence of land use/land cover on climatological values of the diurnal temperature range. *Journal of Climate, 9*, 2941–2944. https://doi.org/10.1175/1520-0442(1996)009%3C2941:TIOLUC%3E2.0.CO;2.

Gaur, A., Eichenbaum, M. K., & Simonovic, S. P. (2018). Analysis and modelling of surface Urban Heat Island in 20 Canadian cities under climate and land-cover change. *Journal of Environmental Management, 206*, 145–157. https://doi.org/10.1016/j.jenvman.2017.10.002.

Guillevic, P. C., Privette, J. L., Coudert, B., Palecki, M. A., Demarty, J., Ottlé, C., et al. (2012). Land Surface Temperature product validation using NOAA's surface climate observation networks—Scaling methodology for the Visible Infrared Imager Radiometer Suite (VIIRS). *Remote Sensing of Environment, 124*, 282–298. https://doi.org/10.1016/j.rse.2012.05.004.

Holderness, T., Barr, S., Dawson, R., & Hall, J. (2013). An evaluation of thermal Earth observation for characterizing urban heatwave event dynamics using the urban heat island intensity metric. *International Journal of Remote Sensing, 34*, 864–884. https://doi.org/10.1080/01431161.2012.714505.

Huong, H. T. L., & Pathirana, A. (2013). Urbanization and climate change impacts on future urban flooding in Can Tho city, Vietnam. *Hydrology and Earth System Sciences, 17*, 379–394. https://doi.org/10.5194/hess-17-379-2013.

Jin, M. L., Dickinson, R. E., & Zhang, D. A. (2005). The footprint of urban areas on global climate as characterized by MODIS. *Journal of Climate, 18*, 1551–1565. https://doi.org/10.1175/JCLI3334.1.

Joshi, R., Raval, H., Pathak, M., Prajapati, S., Patel, A., Singh, V., et al. (2015). Urban heat island characterization and isotherm mapping using geo-informatics technology in Ahmedabad city, Gujarat state, India. *International Journal of Geosciences, 6*, 274. https://doi.org/10.4236/ijg.2015.63021.

Li, F., Liu, H. X., Huisingh, D., Wang, Y. T., & Wang, R. S. (2016). Shifting to healthier cities with improved urban ecological infrastructure: From the perspectives of planning, implementation, governance and engineering. *Journal of Cleaner Production*. https://doi.org/10.1016/j.jclepro.2016.11.151.

Li, W. F., Bai, Y., Chen, Q. W., He, K., Ji, X. H., & Han, C. M. (2014). Discrepant impacts of land use and land cover on urban heat islands: A case study of Shanghai, China. *Ecological Indicators, 47*, 171–178. https://doi.org/10.1016/j.ecolind.2014.08.015.

Mahmood, R., Pielke, R. A., Hubbard, K. G., Niyogi, D., Dirmeyer, P. A., McAlpine, C., et al. (2014). Land cover changes and their biogeophysical effects on climate. *International Journal of Climatology: A Journal of the Royal Meteorological Society, 34*, 929–953. https://doi.org/10.1002/joc.3736.

Melgani, F., & Bruzzone, L. (2004). Classification of hyperspectral remote sensing images with support vector machines. *IEEE Transactions on Geoscience and Remote Sensing, 42*, 1778–1790. https://doi.org/10.1109/TGRS.2004.831865.

Mihalakakou, G., Flocas, H. A., Santamouris, M., & Helmis, C. G. (2002). Application of neural networks to the simulation of the heat island over Athens, Greece, using synoptic types as a predictor. *Journal of Applied Meteorology and Climatology, 41*, 519–527. https://doi.org/10.1175/1520-0450(2002)041%3C0519:AONNTT%3E2.0.CO;2.

Odindi, J. O., Bangamwabo, V., & Mutanga, O. (2015). Assessing the value of urban green spaces in mitigating multi-seasonal urban heat using MODIS Land Surface Temperature (LST) and Landsat 8 data. *International Journal of Environmental of Research, 9*, 9–18.

Oke, T. R. (1995). The heat island of the urban boundary layer: Characteristics, causes and effects. In J. E. Cermak, A. G. Davenport, E. J. Plate, & D. X. Viegas (Eds.). *Wind climate in cities* (pp. 81–107). Dordrecht: Kluwer Academic. https://doi.org/10.1007/978-94-017-3686-2_5.

Oleson, K. W., Bonan, G. B., & Feddema, J. (2010). Effects of white roofs on urban temperature in a global climate model. *Geophysical Research Letters, 37*, L03701. https://doi.org/10.1029/2009GL042194.

Oliveira, S., Andrade, H., & Vaz, T. (2011). The cooling effect of green spaces as a contribution to the mitigation of urban heat: A case study in Lisbon. *Building and Environment, 46*, 2186–2194. https://doi.org/10.1016/j.buildenv.2011.04.034.

Pickett, S. T. A., Cadenasso, M. L., Grove, J. M., Boone, C. G., Groffman, P. M., Irwin, E., et al. (2011). Urban ecological systems: Scientific foundations and a decade of progress. *Journal of Environmental Management, 92*, 331–362. https://doi.org/10.1016/j.jenvman.2010.08.022.

Rizwan, A. M., Dennis, Y. C. L., & Liu, C. H. (2008). A review on the generation, determination and mitigation of Urban Heat Island. *Journal of Environmental Sciences China, 20*, 120–128. https://doi.org/10.1016/S1001-0742(08)60019-4.

Sastry, A., & Barua, D. (2017). Leaf thermotolerance in tropical trees from a seasonally dry climate varies along the slow-fast resource acquisition spectrum. *Scientific Reports, 7*, 11246. https://doi.org/10.1038/s41598-017-11343-5.

Sharifi, E., Sivam, A., & Boland, J. (2016). Resilience to heat in public space: A case study of Adelaide, South Australia. *Journal of Environmental Planning and Management, 59*, 1833–1854. https://doi.org/10.1080/09640568.2015.1091294.

Tan, M. H., & Li, X. B. (2013). Integrated assessment of the cool island intensity of green

spaces in the mega city of Beijing. *International Journal of Remote Sensing, 34*, 3028–3043. https://doi.org/10.1080/01431161.2012.757377.

Theophilou, M. K., & Serghides, D. (2015). Estimating the characteristics of the Urban Heat Island effect in Nicosia, Cyprus, using multiyear urban and rural climatic data and analysis. *Energy and Buildings, 108*, 137–144. https://doi.org/10.1016/j.enbuild.2015.08.034.

Wang, D. D., Morton, D., Masek, J., Wu, A. S., Nagol, J., Xiong, X. X., et al. (2012). Impact of sensor degradation on the MODIS NDVI time series. *Remote Sensing of Environment, 119*, 55–61. https://doi.org/10.1016/j.rse.2011.12.001.

Wilby, R. L. (2003). Past and projected trends in London's urban heat island. *Weather, 58*, 251–260. https://doi.org/10.1256/wea.183.02.

Xian, G., & Crane, M. (2006). An analysis of urban thermal characteristics and associated land cover in Tampa Bay and Las Vegas using Landsat satellite data. *Remote Sensing of Environment, 104*, 147–156. https://doi.org/10.1016/j.rse.2005.09.023.

Xie, Q. J., & Zhou, Z. X. (2015). Impact of urbanization on Urban Heat Island effect based on TM imagery in Wuhan, China. *Environmental Engineering and Management Journal, 14*, 647–655.

Xiong, Y. Z., Huang, S. P., Chen, F., Ye, H., Wang, C. P., & Zhu, C. B. (2012). The impacts of rapid urbanization on the thermal environment: A remote sensing study of Guangzhou, South China. *Remote Sensing, 4*, 2033–2056. https://doi.org/10.3390/rs4072033.

Yuan, F., & Bauer, M. E. (2007). Comparison of impervious surface area and normalized difference vegetation index as indicators of surface urban heat island effects in Landsat imagery. *Remote Sensing of Environment, 106*, 375–386. https://doi.org/10.1016/j.rse.2006.09.003.

Zhang, H., Qi, Z. F., Ye, X. Y., Cai, Y. B., Ma, W. C., & Chen, M. N. (2013). Analysis of land use/land cover change, population shift, and their effects on spatiotemporal patterns of urban heat islands in metropolitan Shanghai, China. *Applied Geography, 44*, 121–133. https://doi.org/10.1016/j.apgeog.2013.07.021.

Zölch, T., Maderspacher, J., Wamsler, C., & Pauleit, S. (2016). Using green infrastructure for urban climate-proofing: An evaluation of heat mitigation measures at the micro-scale. *Urban Forestry & Urban Greening, 20*, 305–316. https://doi.org/10.1016/j.ufug.2016.09.011.